AIAA SciTech Forum
7-11 January 2019, San Diego, California
AIAA Scitech 2019 Forum

10.2514/6.2019-0566

Beneficial Effect of the Coupled Wing-Body Dynamics on Power Consumption in Butterflies

Madhu K. Sridhar[1], Chang-kwon Kang[2], David Brian Landrum[3]
University of Alabama in Huntsville, Huntsville, AL 35899

The incredible migration of Monarch butterflies extends over 4000 km. However, our physical understanding of the aerodynamic mechanisms related to their long-range flight remains inadequate. One of the main challenges is the highly coupled wing-body interactions, resulting in an undulating motion about a mean trajectory. In this study, an analytic expression is derived to quantify the power reduction associated with the wing-body flight dynamics of a butterfly in climbing flight. The model includes a dynamically coupled single mass representing the body and quasi-steady lift, which agrees well with experimental measurements. Our results suggest that the coupled wing-body motion reduces the power consumption compared to a decoupled system. The power consumption is proportional to the square of the Strouhal number and power saving increases with decreasing reduced frequency or decreasing non-dimensional wing loading. The passive reduction in power can potentially enhance the bio-inspired design of long-range Micro-aerial vehicles.

I. Nomenclature

a_z	=	acceleration in the vertical direction	[m/s^2]
$C_{L,\alpha}$	=	lift coefficient due to a mean angle of attack	[1]
$C_{L,wing/body}$, $C_{L,wing}$	=	lift coefficient from coupled and decoupled wing body motion	[1]
$C_{P,wing/body}$, $C_{P,wing}$	=	Power coefficient	[1]
c_m	=	mean chord, $c_m=S/(2R)$	[m]
d	=	migration distance	[m]
$E_{wing/body}$, E_{wing}	=	energy expenditure during migration	[J]
f_w	=	frequency of flapping motion	[1/s]
f_b	=	frequency of body undulation	[1/s]
g	=	acceleration due to gravity	[m/s^2]
h_a	=	plunge amplitude	[m]
k	=	reduced frequency	[1]
$L_{wing/body}$	=	lift corresponding to coupled wing-body motion	[N]
M	=	non-dimensional wing loading	[1]
m	=	butterfly mass	[kg]
P	=	power required	[W]
$\mathbf{p}_{left}$	=	position vector from thorax to left wing	[m]
$\mathbf{p}_{rear}$	=	position vector from thorax to rear wing	[m]
$\mathbf{p}_{right}$	=	position vector from thorax to right wing	[m]
R	=	length of one forewing	[m]
$\hat{r}_2$	=	non-dimensional radius to second moment of wing area	[1]
S	=	total area of left and right forewings	[m^2]
St	=	Strouhal number	[1]
t^*	=	non-dimensional time, $t^*=tf$	[s]
U	=	butterfly velocity magnitude	[m/s]

[1] Graduate Student, Mechanical and Aerospace Engineering, Technology Hall C200, AIAA Student Member.
[2] Assistant Professor, Mechanical and Aerospace Engineering, Technology Hall N266, AIAA Senior Member.
[3] Associate Professor, Mechanical and Aerospace Engineering, Technology Hall N267, AIAA Associate Fellow.

V	=	cruise velocity during migration	[m/s]
A	=	body undulation amplitude	[1]
A_p	=	amplitude associated with C_P	[1]
α	=	pitching angle	[deg]
γ	=	instantaneous angle between the left and right wings	[deg]
γ_{p2p}	=	peak-to-peak angle between the left and right wings	[deg]
θ	=	climb angle	[deg]
ϕ_{exp}	=	experimental phase offset between flapping and body motions	[deg]
ϕ	=	model phase offset between flapping and body motions	[deg]
ϕ_p	=	phase offset associated with C_P	[deg]
ν	=	kinematic viscosity of air	[m^2/s]
ρ	=	air density	[kg/m^3]
ω	=	angular frequency, $\omega=2\pi f$	[rad/s]
$(\dot{\ }), (\ddot{\ })$	=	single and double time derivatives	
$(\bar{\ })$	=	mean quantity	

II. Introduction

LONG distance migration of Monarch butterflies (*Danaus plexippus*) remains one of the unsolved puzzles in the animal kingdom. The aerodynamic mechanisms and power efficiency that enable migrating flight over thousands of kilometers range and up to three months duration are yet to be elucidated. Monarchs are believed to take advantage of favourable atmospheric conditions at higher altitudes to achieve soaring flight but there is a lack of definitive physical models and understanding on what makes this incredible journey possible.

Butterflies are also known to use clap and peel, a variant of clap and fling, wake-capture, leading-edge vortex, and rotational mechanisms [1]. However, compared to the wealth of research on the aerodynamics of insects such as flies [2,3], bees [4,5], dragonflies [6–10], or birds and bats [11], the flight of butterflies remains inadequately understood due to their many unique characteristics. Not only does the Monarch butterfly exhibit the longest range migration, butterflies in general are extremely evasive with agile maneuvers [12–15] and body undulations closely coupled to the wing motions [14,16]. Monarch butterflies have a large pair of flexible, synchronously flapping fore and hind wings attached to a slender segmented body. The combination of large wings and slender body yields the lowest wing loading among the insects [17]. The Monarch butterfly's flight motion is an outcome of the closely coupled wing and body moving at a relatively low frequency of 10 Hz [18]. The trajectories in general are undulating paths about a mean [18].

The body motion can play an important role in the flight of insects and birds. Abdominal motion can benefit short term pitch stability for butterflies in forward flight [19]. Hawkmoths, which are comparable to Monarch butterfly in size, also exhibit abdominal flexion which plays an important role in pitch stability in hover and forward flight [20,21]. The presence of the body can enhance the unsteady lift generation through the nonlinear interaction of the vortex-wake with the body surface [22]. In smaller insects such as fruit flies, the body motion can produce a damping effect in turning [23] and aid in pitch stabilization [24]. In honeybees, reorientation of the abdomen was observed in tethered flight to minimize the aerodynamic drag [25]. Smaller migrating birds such as starlings and finches exhibit undulating flight trajectories known as flap-bounding flight [26]. Flap-bounding flight consists of two phases: ballistic and power phase. In ballistic phase, the wings are folded and remain close to the body and generate no lift whereas in the power phase, the bird flaps its wings. In contrast, Monarch butterflies exhibit a continuous flapping wing motion coupled together with an undulating body motion.

In our earlier study [18], we developed a coupled wing-body model by considering dynamic balance of forces in climbing flight with the butterfly represented as a single mass system that is in dynamic balance with the unsteady aerodynamic forces on the wings. We demonstrated that the predicted body motion closely resembles the experimental measurements of freely flying Monarch butterflies. A key variable in the model is the non-dimensional wing loading: $M = 4m/(\pi\rho c_m S\hat{r}_2^2)$. Here, M is proportional to the butterfly mass m and inversely proportional to fluid density ρ, mean chord length c_m, wing area S, and square of non-dimensional second moment of area of the wing $\hat{r}_2$. We showed that the body undulation amplitude is inversely proportional to M. Smaller insects such as fruit flies and bumblebees have relatively higher M values compared to Monarchs. Correspondingly, the Monarch butterflies exhibit larger body undulation amplitudes.

In this study, we investigate the role of the coupled wing-body dynamics on the power consumption of a Monarch butterfly. We quantify the power associated with an undulating trajectory in climbing flight using our previously developed analytical model [18]. Our preliminary results suggest that the power consumption of the coupled wing-body dynamic system is lower than the power without the wing-body coupling. An aerodynamic model inspired from Monarch butterflies utilizing the power savings from a closely coupled wing body motion can potentially benefit Micro-aerial vehicle (MAV) development.

This abstract is organized as follows. First, we provide a brief description of the methodology focusing on Monarch butterfly morphological and kinematic parameters followed by a summary of the coupled wing-body model from our earlier study [18]. We use this model to derive the power required in a climbing trajectory and compare the power associated with and without body undulation. Finally, we relate the power reduction due to body undulation to non-dimensional parameters.

III. Methodology

A. Morphological Parameters of Monarch Butterflies

Monarch butterflies have a pair of fore and hind wings which synchronously flap during flight. The wings are very large compared to the body. The wings can show significant deformation during flight due to their varying chordwise and spanwise stiffness. Figure 1(a) shows the morphological parameters of a Monarch butterfly relevant to the current study. The wing length of the right forewing R, is defined as the distance between the wing root and the wing tip. The body of the Monarch butterfly is slender and segmented. The total mass of the butterfly is measured for each specimen with the reflective markers attached. In the current study we focus on a representative single butterfly specimen with a wing length of R = 47 mm and a total mass with markers of m = 0.415 g. The non-dimensional radius to the second moment of fore wing area is estimated to be $r_2 = 0.55R$. The morphological parameters and the measured wing kinematic parameters are summarized in Table 1.

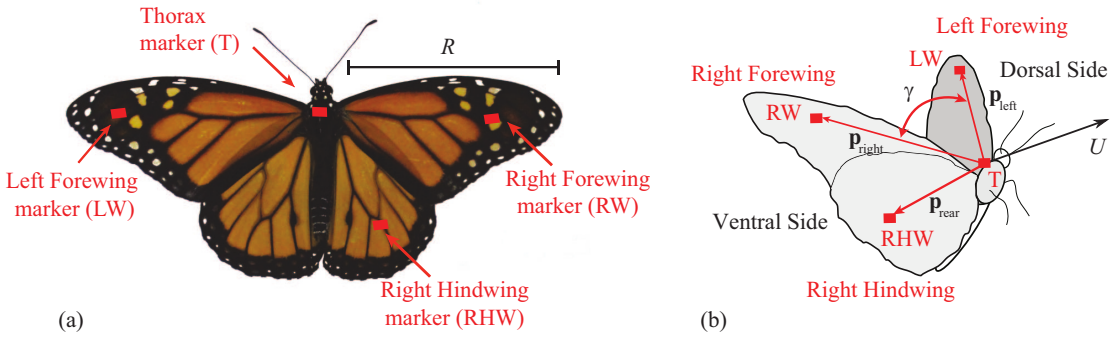

Fig. 1. (a) Marker locations on the body and wings of a Monarch butterfly. The markers are placed on the dorsal and ventral sides of the wing. (b) Schematic showing the definition of the flapping angle γ, defined as the angle between the vectors extending from thorax to the left and the right wing markers.

Table 1. Morphological parameters of the considered Monarch butterfly [18].

Parameter	Value
Butterfly mass with markers, m (g)	0.415
Wing length, R (mm)	47
Non-dimensional radius to the second moment of wing area, $\hat{r}_2$	0.55
Area of left and right forewings, S (mm^2)	19
Mean chord, c_m (mm)	20.2

B. Marker Placement and Data Processing

We measured the wing and body motion by tracking the customized markers placed on the butterfly wing and body. The postprocessing procedure is detailed in our previous work [18]. Here, we provide a brief summary.

VICON motion capture cameras track the motion of customized reflective markers. We used a flat tape reflective marker cut into a small rectangular shape with a dimension 3×5 mm [18]. Each marker weighs 0.0058 g and corresponds to 1.2% of the mass of an average Monarch butterfly. We placed a total of seven markers on each butterfly – six on the wing surfaces and one on the thorax as shown in Fig. 1(a). We placed markers on the dorsal and ventral surfaces of each forewing and one of the hindwings so that the flapping motion would not interfere with the cameras viewing each marker throughout the stroke. The left and right forewings markers, LW and RW, provide data on the flapping angle of the butterfly wing. We use the thorax marker, T, to determine the trajectory.

As shown in Fig. 1(b), three vectors $\mathbf{p}_{\text{left}}$, $\mathbf{p}_{\text{right}}$, $\mathbf{p}_{\text{rear}}$ were defined as extending from the thorax marker to the marker located on each wing. The flapping angle γ, defined here as the angle between both fore wings, was calculated by

$$\gamma = \tan^{-1} \frac{|\mathbf{p}_{\text{left}} \times \mathbf{p}_{\text{right}}|}{\mathbf{p}_{\text{left}} \cdot \mathbf{p}_{\text{right}}}, \tag{1}$$

where γ=0 deg at the end of the upstroke.

We determined the peak-to-peak amplitude of the flapping motion γ_{p2p}, by locating the maximum and minimum value for all the individual cycles in the trajectory. We determined the average of the maximum and minimum flapping angles from all the individual cycles in a trajectory and then calculated the difference between the averages to obtain the peak-to-peak amplitude for the trajectory. The frequency of the flapping angle signal f_w, was calculated using a Fast Fourier Transform (FFT). Finally, we determined the phase ϕ using the complex flapping frequency ϖ, which was obtained from the FFT by

$$\phi = \tan^{-1}\left(\frac{\text{imag } \varpi}{\text{real } \varpi}\right). \tag{2}$$

The VICON motion capture system records the three dimensional position of each marker on the butterfly. A sampling rate of 100 Hz was used in recording the marker data. A sampling rate of 100 Hz corresponds to nearly ten times the characteristic flapping frequency of Monarch butterflies [18]. The data is filtered using a low pass filter with a cutoff frequency of 50 Hz.

Figure 2(a) shows the three dimensional position of the thorax and the wing markers for ten consecutive flapping cycles in a climbing trajectory. We consider the trajectory from flight 1372, butterfly #55 from the experimental measurements from our earlier study [18]. The three dimensional variation of the fore wing markers relative to the thorax can be observed in Fig. 2(a). The trajectory of the butterfly is defined as the position of the thorax marker T, during flight. The trajectory of the butterfly shows an undulating variation about a mean trajectory. The climb angle of the trajectory with the horizontal plane is θ = 24.2 deg based on the end points of the trajectory. The vertical position of the thorax and wing markers is shown in Fig. 2(b). The average climb rate of the trajectory is calculated from the altitudes of the end points of the trajectory over time and corresponds to 0.76 m/s. The instantaneous velocity of the thorax marker is obtained by differentiating it with respect to time. Figure 2(c) shows the variation of the thorax velocity magnitude for the trajectory shown in Fig 2(b) with a mean velocity magnitude, U = 1.88 m/s.

The position of the thorax and wing markers is used with Eq. (1) to determine the flapping angle γ, between the left and the right forewings. Figure 2(d) shows that the variation of the normalized flapping angle is nearly sinusoidal. The flapping angle is close to γ = 0 deg when the wings are folded above the body near the beginning of the downstroke. At the end of the downstroke, the flapping angle is close to γ = 300 deg. The undulation of the thorax about the mean trajectory is obtained by detrending the vertical position of the thorax with a moving average filter. The resulting normalized undulation is shown in Fig. 2(d). The body undulation frequency f_b, is obtained by taking the FFT of the undulating motion about the mean trajectory. The flapping motion and body undulation shown in Fig. 2(d) share the same frequency, i.e. $f_w = f_b = f$ = 9.9 Hz, suggesting that the wing motion and the body motion are closely coupled to each other. The body of the butterfly rises up during the downstroke and then falls during the upstroke resulting in a undulating motion with a constant phase offset with the wing motion. The wing-body phase offset ϕ_{exp}, shown in Fig. 2(d) is determined from Eq. (2) as ϕ_{exp} = 94.3 deg. Table 2 gives a summary of the body and wing kinematics parameters corresponding to the trajectory shown in Fig. 2.

The body and the wing motion are closely coupled. In our earlier work [18] we developed an analytical model which explains this dynamic relationship and is discussed in Section III.C.

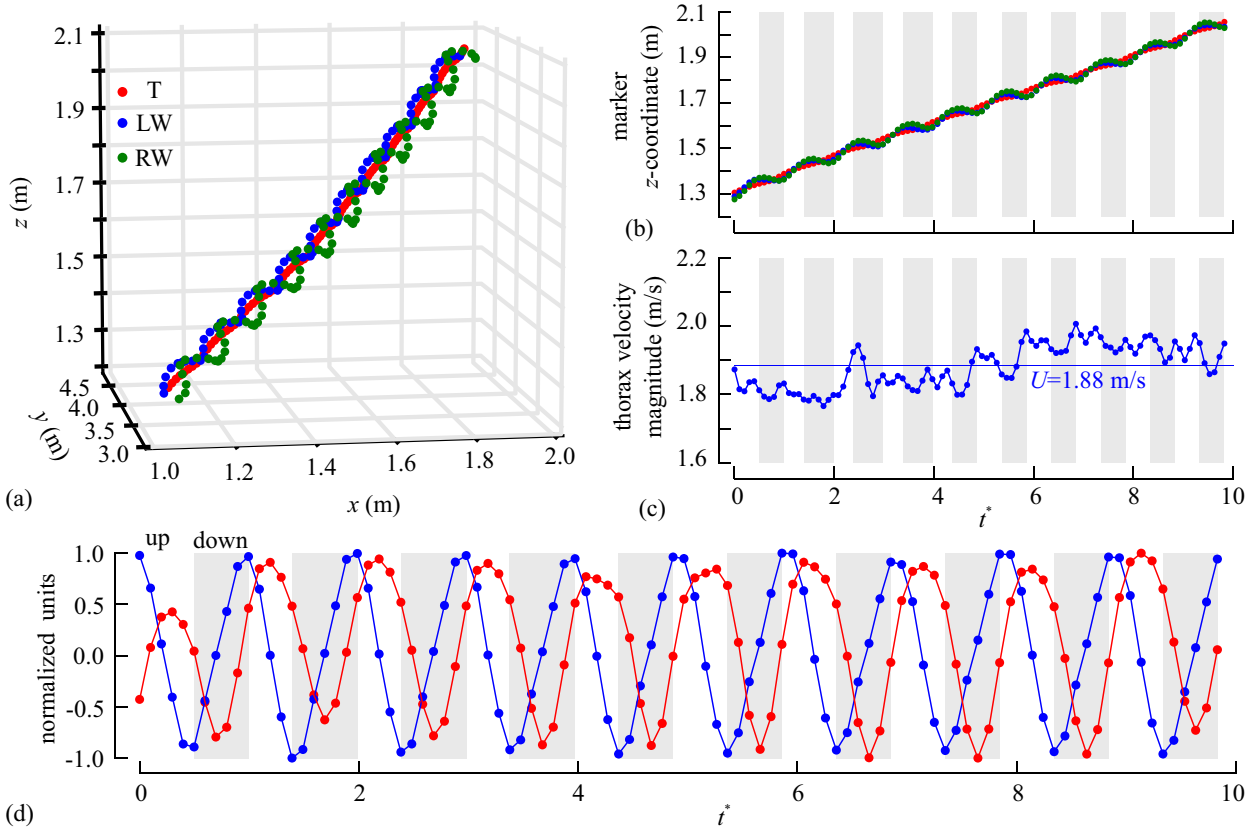

Fig. 2. (a) Three dimensional recorded position of thorax and wing markers in a climbing trajectory for ten flapping cycles. Thorax marker T, is shown in red and left wing, LW and right wing RW, markers are shown in blue and green, respectively. The thorax has a climb angle of θ = 24.2 deg with the horizontal plane. (b) The *z*-component of three markers in (a) with respect to non-dimensional time. The thorax trajectory has a vertical climb rate of 0.76 m/s. (c) Variation of thorax velocity magnitude. The average value over ten cycles is *U* = 1.88 m/s. (d) Comparison of undulating motion of the body and flapping motion of the wing. The undulating motion of the body (red) and flapping angle γ (blue) are normalized. The trajectory is taken from the experimental measurements from our earlier study [18]. Downstroke is shaded.

C. Dynamic Relationship between Wing Motion and Body Undulation

In our earlier work [18], we modeled the dynamic relationship between wing and body motion by considering the butterfly as a single mass system with unsteady aerodynamic forces on the wing. We considered the butterfly as a single mass system climbing at an angle θ and used balance of forces to obtain

$$ma_z = L_{wing/body} - mg\cos\theta\,, \tag{3}$$

where a_z is the acceleration normal to the instantaneous velocity, g is the gravitational acceleration, and $L_{wing/body}$ is the lift force normal to the mean climbing trajectory corresponding to a coupled wing-body motion. The flapping motion of the wing was modeled with a two dimensional plunge approximation as

$$h(t) = -h_a\cos(2\pi ft)\,, \tag{4}$$

where $h_a = \gamma_{p2p}R\hat{r}_2/4$ is the plunge amplitude. In Eq. (4) the plunge motion is considered in the downward direction. Three dimensional rotating wing motion about the wing root is converted to a two dimensional motion by considering wing plunge at the second moment of area of the wing at a distance of $\hat{r}_2R$ from the wing root. We

considered the unsteady lift acting on the butterfly using Theodorsen's lift equation in the quasi-steady limit [27], which can be written as

$$L_{wing/body} = \frac{1}{2}\rho U^2 S\hat{r}_2^{\,2} C_{L,wing/body} = \frac{1}{2}\rho U^2 S\hat{r}_2^{\,2}\left(\frac{\pi c_m}{2U^2}(\ddot{z}-\ddot{h})+\frac{2\pi}{U}(\dot{z}-\dot{h})+C_{L,\alpha}\right). \tag{5}$$

Here, ρ is the fluid density and the area of the left and right forewings S is multiplied by $\hat{r}_2$ to scale the magnitude of the aerodynamic forces on a rotating flapping wing of an insect to a plunging airfoil as modeled by Theodorsen [28–30]. Since many butterflies cannot actively control their pitch angle due to structural constraints [31,32], we neglect the lift terms due to pitch velocity and acceleration in Eq. (5). We modeled the two-way coupled dynamics between the wing and body motion by adjusting the plunge motion with instantaneous body motion z, in Eq. (5). The first and second terms in Eq. (5) correspond to the circulatory and non-circulatory terms, respectively. The third term in Eq. (5) is the stationary lift term modeled by $C_{L,\alpha} = 2\pi\alpha$. This corresponds to the lift component that offsets the weight component $mg\cos\theta$ as shown in Fig. 3(a). The butterfly climb follows a straight trajectory when it maintains a mean angle of attack of $\alpha = mg\cos\theta/(\pi\rho U^2 S\hat{r}_2^{\,2})$.

The solution to Eq. (5) is [18]

$$\frac{z(t)}{h_a} = \mathrm{A}\{\cos(2\pi ft+\phi)-\cos\phi\}, \tag{6}$$

where the non-dimensional undulation amplitude A and phase offset ϕ are given respectively as

$$\mathrm{A} = \frac{C_1}{1+\left(\frac{k}{2}(M-1)\right)^2}\sqrt{1+\left(\frac{kM}{2C_1}\right)^2}; \qquad \phi = \arctan\left(\frac{kM}{2C_1}\right), \tag{7}$$

Here, the coefficient $C_1 = (M\text{-}1)(k/2)^2\text{-}1$, the reduced frequency is $k = \pi f c_m/U$, and, again, the factor M is the non-dimensional wing loading. The model parameters from Eqs. (6) and (7) are summarized in Table 2.

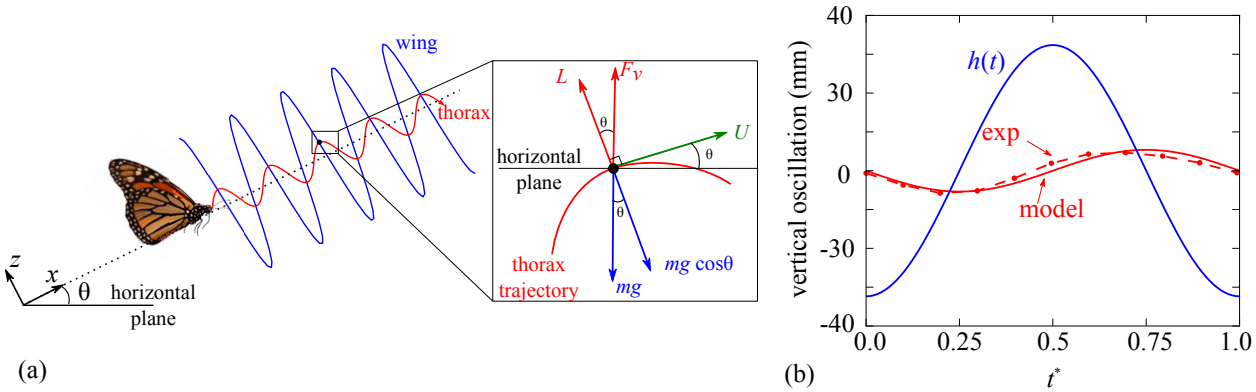

Fig. 3. (a) Schematic showing the forces acting on a butterfly in a climbing trajectory. F_v is the vertical force acting in the direction opposite to butterfly weight. The direction of the instantaneous thorax velocity is given by U. The component of force normal to the instantaneous velocity is the lift, L. (b) Comparison of the undulating body motion from the experimental measurements (first cycle) and model (Eq. (6)). The plunge motion, $h(t)$ is also shown. The experimental measurements are from our earlier study [18].

Table 2. Kinematic parameters from the trajectory in Fig. 2 and the corresponding parameters from the coupled wing-body model. Experimental measurements are from our earlier study [18].

Parameter	Value
Plunge amplitude, h_a (mm)	32.36
Exp. body undulation amplitude (mm)	6.6
Exp. phase offset, ϕ_{exp} (deg)	94.3
Flapping amplitude, γ_{p2p} (deg)	286.9
Body undulation frequency, f_b (Hz)	9.9
Mean forward velocity of thorax, U (m/s)	1.88
Reduced frequency, k	0.33
Non-dimensional wing loading, M	37.13
$C_1 = (M\text{-}1)(k/2)^2\text{-}1$	0.0115
Model body undulation amplitude, Ah_a (mm)	5.4
Model phase offset, ϕ (deg)	89.9

IV. Results and Discussion

A. Derivation of the Power for the Dynamically Coupled Wing-Body Butterfly Model

The instantaneous position of the body is given by Eq. (6). The corresponding velocity and acceleration of the body are

$$\dot{z}(t) = -\mathrm{A}h_a\omega\sin(\omega t+\phi); \quad \ddot{z}(t) = -\mathrm{A}h_a\omega^2\cos(\omega t+\phi)\,, \tag{8}$$

where $\omega = 2\pi f$ is the angular frequency of the body undulation and A and ϕ are the non-dimensional amplitude and phase offset given in Eq. (7). Substituting the velocity and acceleration associated with the plunging motion of the wing given by Eq. (4) and the undulating motion of the body given by Eq. (6) into Eq. (5), and then nondimensionalizing, yields the lift coefficient for the coupled wing-body motion as

$$\begin{aligned} C_{L,wing/body}(t) = \frac{\pi c_m}{2U^2}\{-\mathrm{A}h_a\omega^2\cos(\omega t+\phi) - h_a\omega^2\cos(\omega t)\} + \\ \frac{2\pi}{U}\{-\mathrm{A}h_a\omega\sin(\omega t+\phi) - h_a\omega\sin(\omega t)\} + C_{L,\alpha}\,. \end{aligned} \tag{9}$$

For the case where the wing and body motions are decoupled from each other, the body undulation amplitude becomes zero and the lift coefficient without the wing-body coupling reduces to

$$C_{L,wing}(t) = \frac{\pi c_m}{2U^2}\{-h_a\omega^2\cos(\omega t)\} + \frac{2\pi}{U}\{-h_a\omega\sin(\omega t)\} + C_{L,\alpha}\,. \tag{10}$$

The power coefficient for the coupled wing body motion can be defined as

$$C_{P,wing/body} = C_{L,wing/body}\left(\frac{-\dot{h}}{U}\right), \tag{11}$$

where $\dot{h}(t) = 2\pi f h_a\sin(2\pi f t)$ is the plunge velocity of the wing. It is also useful to calculate the mean coefficient of power for the coupled motion in a cycle from Eq. (11) as

$$\bar{C}_{P,wing/body} = f \int_0^{1/f} C_{P,wing/body}(t)dt. \tag{12}$$

Determining the power expenditure during flapping flight can provide an estimate of the energetic costs associated with the flight. Substituting the lift coefficient from Eq. (9) in Eq. (12) results in

$$\begin{aligned}\bar{C}_{P,wing/body} = {} & \frac{\pi c_m f A h_a^2}{2U^3}\left[\int_0^{1/f} \omega^3 \cos(\omega t+\phi)\sin(\omega t)dt + \int_0^{1/f} \omega^3 \cos(\omega t)\sin(\omega t)dt\right] \\ & + \frac{2\pi f A h_a^2}{U^2}\left[\int_0^{1/f} \omega^2 \sin(\omega t+\phi)\sin(\omega t)dt + \int_0^{1/f} \omega^2 \sin(\omega t)\sin(\omega t)dt\right] \\ & - \frac{f h_a C_{L,\alpha}}{U}\int_0^{1/f} \omega \sin(\omega t)dt.\end{aligned} \tag{13}$$

The integrals in Eq. (13) can be exactly evaluated and simplified to

$$\bar{C}_{P,wing/body} = \frac{-4A\pi^3 f^2 h_a^2}{U^2}\sqrt{\left(\frac{k}{2}\right)^2+1}\,\sin\left(\phi - \arctan\left(\frac{2}{k}\right)\right) + \frac{4\pi^3 f^2 h_a^2}{U^2}. \tag{14}$$

Equation (14) quantifies the mean coefficient of power associated with a coupled wing-body motion. If the influence of the body undulation on the lift is neglected in Eq. (5), resulting in a lift coefficient given by Eq. (10), the power coefficient reduces to the third term in Eq. (14): $\bar{C}_{P,wing} = 4\pi^3 f^2 {h_a}^2/U^2$. The relationship between the wing-body coupling and the associated lift and power is discussed in the Section IV.B.

B. Power Reduction from the Wing-Body Coupling

Equation (14**)** represents the mean power coefficient for a coupled wing-body motion where $\bar{C}_{P,wing} = 4\pi^3 f^2 {h_a}^2/U^2$ corresponds to the power due to the flapping motion of the wing. The mean lift and power with and without wing-body coupling based on the morphological parameters given in Table 1 and kinematic parameters in Table 2 are shown in Table 3. The amplitude and phase associated with C_P for the trajectory in Fig. 2 are A_p = 0.6 and ϕ_p = 80.53 deg, respectively.

Table 3. Mean lift and power with and without wing-body coupling.

Parameter	Value
Mean C_L for coupled wing-body motion, $\bar{C}_{L,wing/body}$	2.96
Mean C_L for purely plunging motion, $\bar{C}_{L,wing}$	2.96
Mean C_P for coupled wing-body motion, $\bar{C}_{P,wing/body}$	3.49
Mean C_P for purely plunging motion, $\bar{C}_{P,wing}$	3.58
Strouhal number, $St=2fh_a/U$	0.34
Amplitude associated with C_P, A_p	0.6
Phase offset associated with C_P, ϕ_p (deg)	80.53

Figure 4(a) shows the variation of the normalized body and plunge motion and the corresponding plunge velocity in a cycle. The resulting time history of the lift coefficient with and without coupled body motion is shown in Fig. 4(b). The influence of the wing-body coupling on the mean lift is negligible. A slight offset is observed between the two profiles. On the other hand, the differences in the corresponding power coefficient for the two cases is noticeable as shown in Fig. 4(c). The C_P profile consists of two peaks during a flapping cycle of the wing with a higher peak observed during the second half of the cycle. Although the $C_{P,wing/body}$ is not consistently lower than the $C_{P,wing}$ throughout the cycle, the mean $\bar{C}_{P,wing/body}$ = 3.49 is slightly (around 3%) lower than the $\bar{C}_{P,wing}$= 3.58 (Table 3). The main reason is that the lift coefficient with the wing-body coupling peaks earlier. This phase difference results in the lower mean power with the wing-body coupling.

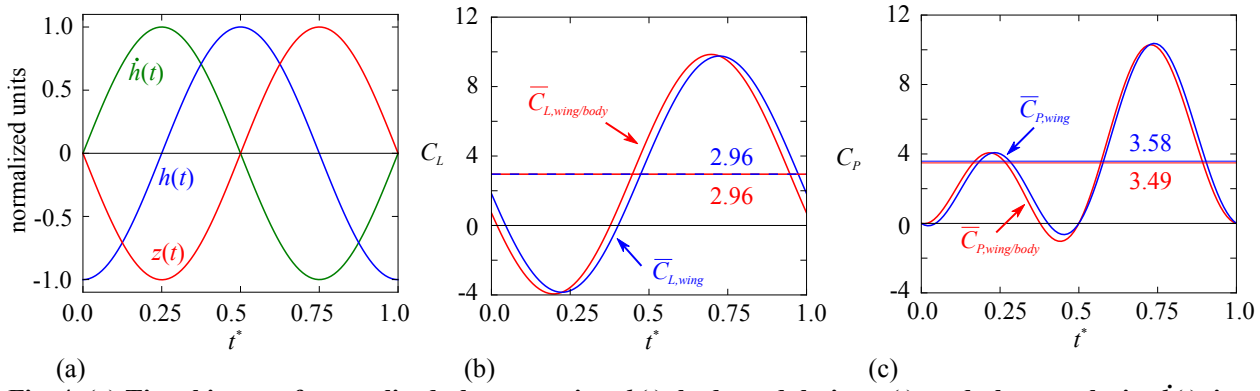

Fig. 4. (a) Time history of normalized plunge motion, $h(t)$, body undulation, $z(t)$, and plunge velocity $\dot{h}(t)$, in a flapping cycle. (b) Variation of C_L in a flapping cycle for a coupled wing-body motion and purely plunging wing motion. Mean C_L for the two profiles over a flapping cycle is shown. (c) Variation of C_P in a flapping cycle highlighting the difference between a coupled wing-body motion and purely plunging wing motion. Mean C_P over a flapping cycle is shown.

C. Analysis of the Power Reduction associated with the Wing-Body Coupling

The lift and power coefficient in Eqs. (9) and (14) can be rewritten in terms of the non-dimensional parameters that are widely used in bioinspired flight dynamics [11] as

$$\overline{C}_{P,wing/body} = -\mathrm{A_p} St^2 \sin(\phi - \phi_\mathrm{p}) + \pi^3 St^2, \tag{15}$$

where the amplitude can be rewritten as $\mathrm{A_p} = \pi^3 \mathrm{A}\sqrt{(k/2)^2 + 1}$ and the phase is $\phi_\mathrm{p} = \arctan(2/k)$. The Strouhal number corresponding to the flapping motion is defined as $St = 2h_a f/U$. The square of the Strouhal number appears as a common factor. The reduced frequency is again $k = \pi f c_\mathrm{m}/U$. A is the non-dimensional body undulation amplitude (Eq. (7)), ϕ is the phase offset between body and wing motion (Eq. (7)).

The first term on the RHS in Eq. (15) corresponds to the power reduction due to the wing-body coupling and undulation. The second term $\overline{C}_{P,wing} = \pi^3 St^2$ corresponds to the intrinsic power due to the flapping motion of the wing, which is always positive.

The overall power can be reduced due to a coupled wing-body motion when the first term on the RHS in Eq. (14) becomes negative. In other words, if $\mathrm{A_p} St^2 \sin(\phi - \phi_\mathrm{p}) > 0$, we have power savings due to the body undulation. We solve this inequality by inserting the definitions of ϕ in Eq. (7) and $\phi_\mathrm{p} = \arctan(2/k)$, yielding

$$\sin\left(\arctan\left(\frac{kM}{2C_1}\right) - \arctan\left(\frac{2}{k}\right)\right) < 0\,. \tag{16}$$

The solution to the above inequality is $k^2 > -4$, which implies that there is always a reduction in power due to the wing-body coupling.

The magnitude of the power reduction normalized by St^2, which is $\mathrm{A_p}$, depends on the reduced frequency k, and the non-dimensional wing loading M. The ranges of values for M, St and k relevant to the considered Monarch butterflies are $30 < M < 50$, $0.16 < St < 0.22$ and $0.24 < k < 0.46$, respectively [18]. Based on this observation, we focus on the influence of M and k on the power reduction normalized by St^2 and corresponding to the trajectory in Fig. 2. The variation of $\mathrm{A_p}\sin(\phi - \phi_\mathrm{p})$ as a function of k and M is shown in Fig. 5. The amount of power reduction observed is higher in the region of lower M and k. For a given k, as the magnitude of M increases, $\mathrm{A_p}\sin(\phi - \phi_\mathrm{p})$ approaches zero. The range of reduced frequencies and non-dimensional wing loading recorded from all the flights is highlighted in Fig. 5 in blue. The domain given by the intersection of the bounds of k and M in Fig. 5 indicates the range of power savings associated with Monarch butterfies.

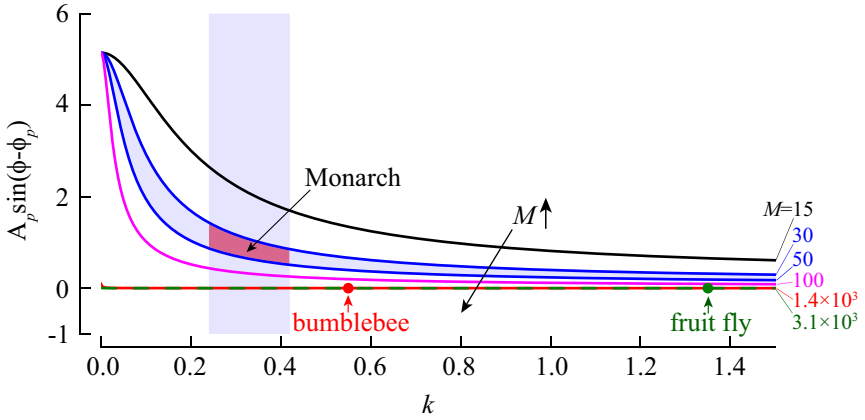

Fig. 5. Power reduction $A_p\sin(\phi-\phi_p)$ as a function of reduced frequency k and non-dimensional wing loading M. The range of k and M for Monarch butterflies [18] is highlighted in blue. The domain of intersection of k and M denotes the range of power savings for Monarch butterflies.

Figure 5 also shows the regimes corresponding to smaller insects such as fruit flies and bumblebees which exhibit much higher non-dimensional wing loadings compared to Monarch butterflies [18]. Fruit flies have a non-dimensional wing loading of $M = 3.1\times10^3$ and bumblebees have $M = 1.4\times10^3$ [18], which are two orders of magnitude higher than for Monarchs. Additionally, the reduced frequency for fruit flies and bumblebees is $k = 1.35$ and $k = 0.55$, respectively. Because of the higher non-dimensional wing loading M for fruit flies and bumblebees, the body undulation amplitudes are much lower than Monarchs. Our results summarized in Table 4 suggest that the corresponding power savings for these insects due to body undulation are negligible compared to Monarch butterflies.

Table 4. Comparison of non-dimensional variables and power savings for Monarch, bumblebee [18] and fruit fly [18,33]**.**

Parameter	Monarch	Bumblebee	Fruit fly
Non-dimensional wing loading, M	37.13	1.4×10^3	3.1×10^3
Reduced frequency, k	0.33	0.55	1.35
Strouhal number, St	0.34	0.59	1.72
Body undulation amplitude (mm)	5.37	0.02	5.2×10^{-4}
Power saving, $A_p\sin(\phi-\phi_p)$	0.81	2.2×10^{-4}	3.3×10^{-6}

D. Comparison of Power Expenditure with and without Body Undulation

As discussed in Section IV.B, the trajectory with a coupled wing-body motion yields a lower mean power coefficient. The effect of lower power expenditure due to body undulation in a long distance migrating flight can be estimated in terms of the energy consumption based on a typical Monarch specimen: $\bar{C}_{P,wing/body} = 3.49$ and $\bar{C}_{P,wing} = 3.58$. The corresponding power with and without coupled body motion are given by $P_{wing/body} = 4.382$ mW and $P_{wing} = 4.505$ mW, respectively. The body undulation reduces the mean power by 0.123 mW, or around 3%.

We can define the total energy expenditure during the migration distance as $E = Pd/V$, where P is the power required, d is the migration distance and V is an average cruise velocity. If we assume a constant cruise speed of $V = 5$ m/s during migration [34], it takes around 222 hours (9.3 days) for the Monarchs to migrate a distance of $d = 4000$ km without stops. The energy expenditure over the migration distance with and without body undulation assuming a constant cruise velocity is $E_{wing/body} = 3.479\times10^4$ J and $E_{wing} = 3.578\times10^4$ J, respectively. The body undulation decreases the energy expenditure by around 3%. A typical Monarch weighing 600 mg contains about 23% (140 mg) of fat [34]. Based on the metabolic rate measured for the Painted lady butterfly, Gibo and Pallet [34] report that a typical Monarch butterfly will consume fat at the rate of 13 mg/hr (120 cal/hr). Based on these energy estimates, assuming that a Monarch constantly replenishes its fat reserve during migration, energy saving of 3% due to an undulating body trajectory could extend the total flight time by about 2 flight hours or about 36 km (0.9% d) range with a constant cruise velocity compared to a purely uncoupled wing motion. Migration is energetically expensive [35] and Monarch butterflies expend lipid reserves during migration in spite of possible intermittent

feeding on nectar along the way [35]. Though small, energy saving resulting from body undulation can potentially be crucial for long distance migration of Monarchs.

V. Concluding Remarks

Monarch butterflies are highly maneuverable and exhibit wing motions coupled with undulating body motion. The purpose and the role of body undulation are not clearly understood. In this work, we express the Monarch power expenditure for a coupled wing-body motion in a climbing trajectory. The butterfly is considered as a single mass system and the aerodynamic lift acting on the butterfly is modelled using the unsteady Theodorsen's equation.

We derived an analytical expression for the coefficient of power due to coupled wing-body motion. We compared the power savings from the model to a decoupled wing motion. The results indicate that the mean lift coefficients of the coupled wing-body motion and decoupled wing motion are similar. However, the power coefficient is slightly lower for the coupled wing-body motion.

We also expressed the power saving in terms of non-dimensional parameters and identified the range relevant for Monarch butterflies over which power saving is observed. The amount of power reduction observed is higher for lower non-dimensional wing loading and reduced frequency. For the trajectory considered in this study, inclusion of the body motion reduced the total power consumption by around 3%. For a typical Monarch butterfly weighing around 600 mg and migrating over 4000 km, the estimated energy saving due body undulation could extend the total flight time by 2 hours or by 36 km range compared to a purely uncoupled wing motion.

The current study provides a novel analytical framework to describe the role of body undulation in Monarch butterfly flight. Understanding the role of body undulation in power savings can be beneficial in developing long range MAVs.

The current study is based on quasi-steady, two dimensional, single mass butterfly model. In the future, modeling based on high fidelity Navier-Stokes simulation including the effects of wing flexibility will be considered. In addition, assessment of the power expenditure in Monarch butterflies based on the relative motion of thorax and abdomen segments will be considered. The analytical model of power estimation from coupled wing-body motion presented in the current study will be evaluated based on a statistically significant number of experimental measurements of Monarch butterflies in free flight.

Acknowledgments

This work is partly supported by CBET-1335572 and CMMI-1761618.

References

[1] Srygley, R. B., and Thomas, A. L. R., "Unconventional Lift-Generating Mechanisms in Free-Flying Butterflies," *Nature*, Vol. 420, 2002, pp. 487–489.

[2] Dickinson, M. H., Lehmann, F.-O., and Sane, S. P., "Wing Rotation and the Aerodynamic Basis of Insect Flight," *Science*, Vol. 284, Nr. 5422, 1999, pp. 1954–1960.

[3] Muijres, F. T., Elzinga, M. J., Melis, J. M., and Dickinson, M. H., "Flies Evade Looming Targets by Executing Rapid Visually Directed Banked Turns," *Science*, Vol. 344, Nr. April, 2014, pp. 172–178.

[4] Dillon, M. E., and Dudley, R., "Surpassing Mt. Everest: Extreme Flight Performance of Alpine Bumble-Bees," *Biology Letters*, Vol. 10, Nr. 2, 2014, p. 20130922.

[5] Mountcastle, A. M., Combes, S. a, and Mountcastle, A. M., "Wing Flexibility Enhances Load-Lifting Capacity in Bumblebees.," *Proceedings. Biological Sciences / The Royal Society*, Vol. 280, Nr. 1759, 2013, p. 20130531.

[6] Wang, Z. J., "Dissecting Insect Flight," *Annual Review of Fluid Mechanics*, Vol. 37, Nr. 1, 2005, pp. 183–210.

[7] Jongerius, S. R., and Lentink, D., "Structural Analysis of a Dragonfly Wing," *Experimental Mechanics*, Vol. 50, Nr. 9, 2010, pp. 1323–1334.

[8] Wang, Z. J., and Russell, R. D., "Effect of Forewind and Hindwing Interactions on Aerodynamic Forces and Power in Hovering Dragonfliy Flight," *Physical Review Letters*, Vol. 99, 2007, p. 148101.

[9] Alexander, D. E., "Unusual Phase Relationships between the Forewing and Hindwings in Flying Dragonflies," *Journal of Experimental Biology*, Vol. 109, 1984, pp. 379–383.

[10] Wang, J. K., and Sun, M., "A Computational Study of the Aerodynamics and Forewing-Hindwing Interaction of a Model Dragonfly in Forward Flight.," *The Journal of Experimental Biology*, Vol. 208, 2005, pp. 3785–3804.

[11] Shyy, W., Aono, H., Kang, C., and Liu, H., *An Introduction to Flapping Wing Aerodynamics*, Cambridge University Press, New York, 2013.

[12] Dudley, R., "Biomechanics of Flight in Neotropical Butterflies: Aerodynamics and Mechanical Power Requirements," *Journal of Experimental Biology*, Vol. 357, Nr. 1, 1991, pp. 335–357.

[13] Thomas, A. L. R., Taylor, G. K., Srygley, R. B., Nudds, R. L., and Bomphrey, R. J., "Dragonfly Flight: Free-Flight and

Tethered Flow Visualizations Reveal a Diverse Array of Unsteady Lift-Generating Mechanisms, Controlled Primarily via Angle of Attack.," *The Journal of Experimental Biology*, Vol. 207, 2004, pp. 4299–4323.
[14] Srygley, R. B., "Locomotor Mimicry in Butterflies? The Associations of Positions of Centres of Mass among Groups of Mimetic, Unprofitable Prey," *Philosophical Transactions: Biological Sciences*, Vol. 343, Nr. 1304, 1994, pp. 145–155.
[15] Dudley, R., and Srygley, R., "Flight Physiology of Neotropical Butterflies: Allometry of Airspeeds During Natural Free Flight," *Journal of Experimental Biology*, Vol. 191, Nr. 1, 1994, pp. 125–39.
[16] Lin, T., Zheng, L., Hedrick, T., and Mittal, R., "The Significance of Moment-of-Inertia Variation in Flight Manoeuvres of Butterflies," *Bioinspiration & Biomimetics*, Vol. 7, Nr. 4, 2012, p. 044002.
[17] Tennekes, H., *The Simple Science of Flight: From Insects to Jumbo Jets*, MIT Press, Cambridge, 2009.
[18] Kang, C., Cranford, J., Sridhar, M. K., Kodali, D., Landrum, D. B., and Slegers, N., "Experimental Characterization of a Butterfly in Climbing Flight," *AIAA Journal*, Vol. 56, Nr. 1, 2017, pp. 15–24.
[19] Jayakumar, J., Senda, K., and Yokoyama, N., "Control of Pitch Attitude by Abdomen During Forward Flight of Two-Dimensional Butterfly," *Journal of Aircraft*, 2018, pp. 1–11.
[20] Cheng, B., Deng, X., and Hedrick, T. L., "The Mechanics and Control of Pitching Manoeuvres in a Freely Flying Hawkmoth (Manduca Sexta)," *Journal of Experimental Biology*, Vol. 214, 2011, pp. 4092–4106.
[21] Dyhr, J. P., Morgansen, K. A., Daniel, T. L., and Cowan, N. J., "Flexible Strategies for Flight Control : An Active Role for the Abdomen," *Journal of Experimental Biology*, Vol. 216, 2013, pp. 1523–1536.
[22] Liu, G., Dong, H., and Li, C., "Vortex Dynamics and New Lift Enhancement Mechanism of Wing – Body Interaction in Insect Forward Flight," *Journal of Fluid Mechanics*, Vol. 795, 2016, pp. 634–651.
[23] Cheng, B., Fry, S. N., Huang, Q., and Deng, X., "Aerodynamic Damping during Rapid Flight Maneuvers in the Fruit Fly Drosophila," *The Journal of Experimental Biology*, Vol. 213, 2010, pp. 602–612.
[24] Ristroph, L., Ristroph, G., Morozova, S., Bergou, A. J., Chang, S., Wang, Z. J., Cohen, I., Ristroph, L., Ristroph, G., Morozova, S., Bergou, A. J., Chang, S., Guckenheimer, J., Wang, Z. J., and Cohen, I., "Active and Passive Stabilization of Body Pitch in Insect Flight Active and Passive Stabilization of Body Pitch in Insect Flight," *Journal of Royal Society Interface*, Vol. 10, 2013, p. 20130237.
[25] Luu, T., Cheung, A., Ball, D., and Srinivasan, M. V, "Honeybee Flight : A Novel ' Streamlining ' Response," *The Journal of Experimental Biology*, Vol. 214, 2011, pp. 2215–2225.
[26] Pennycuick, C. J., "Speeds and Wingbeat Frequencies of Migrating Birds Compared with Calculated Benchmarks," *Journal of Experimental Biology*, Vol. 3294, 2001, pp. 3283–3294.
[27] Theodorsen, T., "General Theory of Aerodynamic Instability and the Mechanism of Flutter," *NACA Report*, Nr. 496, 1935.
[28] Han, J., Kim, J., Chang, J. W., and Han, J., "An Improved Quasi-Steady Aerodynamic Model for Insect Wings That Considers Movement of the Center of Pressure," *Bioinspiration & Biomimetics*, Vol. 10, 2015, p. 046014.
[29] Lua, K.B., Lim, T.T., Yeo, K. S., "Scaling of Aerodynamic Forces of Three-Dimensional Flapping Wings," *AIAA Journal*, Vol. 52, Nr. 5, 2014, pp. 1095–1101.
[30] Ellington, C. P., "The Aerodynamics of Hovering Insect Flight II. Morphological Parameters," *Philosophical Transactions of the Royal Society of London Series B-Biological Sciences*, Vol. 305, Nr. 1122, 1984, pp. 17–40.
[31] Fei, Y. H. J., and Yang, J. T., "Importance of Body Rotation During the Flight of a Butterfly," *Physical Review E*, Vol. 93, Nr. 3, 2016, p. 033124.
[32] Tanaka, H., and Shimoyama, I., "Forward Flight of Swallowtail Butterfly with Simple Flapping Motion," *Bioinspiration & Biomimetics*, Vol. 5, Nr. 2, 2010, p. 26003.
[33] Ristroph, L., Bergou, A. J., Guckenheimer, J., Wang, Z. J., and Cohen, I., "Paddling Mode of Forward Flight in Insects," Vol. 178103, Nr. April, 2011, pp. 1–4.
[34] Gibo, D. L., and Pallet, M. J., "Soaring Flight of Monarch Butterflies, Danaus Plexippus (Lepidoptera: Danaidae), During the Late Summer Migration in Southern Ontario," *Canadian Journal of Zoology*, Vol. 57, Nr. 7, 1979, pp. 1393–1401.
[35] Alonso-Mejia, A. A., Rendon-Salinas, E., Montesinos-Patino, E., and Brower, L. P., "Use of Lipid Reserves by Monarch Butterflies Overwintering in Mexico: Implications for Conservation," *Ecological Applications*, Vol. 7, Nr. 3, 1997, pp. 934–947.